

# Effect of LiNbO<sub>3</sub> polarity on the structural, optical and acoustic properties of epitaxial ZnO and Mg<sub>x</sub>Zn<sub>1-x</sub>O films

Sabina Kuprenaite,<sup>1</sup> Samuel Margueron,<sup>\*1</sup> Marina Raschetti,<sup>1</sup> Cyril Millon,<sup>1</sup> Thomas Baron,<sup>1</sup> William Daniau,<sup>1</sup> Sylvain Ballandras,<sup>2</sup> Brice Gautier,<sup>3</sup> David Albertini,<sup>3</sup> Pascal Boulet,<sup>4</sup> and Ausrine Bartasyte<sup>1</sup>

<sup>1</sup> *FEMTO-ST Institute, University of Bourgogne Franche-Comté, CNRS (UMR 6174), ENSMM, 26 rue de l'Épitaphe, 25030, Besançon, France*

<sup>2</sup> *freq|n|sys SAS, 18 Rue Alain Savary, 25000 Besançon, France*

<sup>3</sup> *Institut des Nanotechnologies de Lyon, INSA de Lyon, Université de Lyon, UMR CNRS 5270, 7, avenue Capelle, F-69621 Villeurbanne, France*

<sup>4</sup> *Jean Lamour Institute, CNRS (UMR 7198), Université de Lorraine, 2 allée André Guinier*

*Campus Artem, 54000 Nancy, France*

## Abstract

The effect of LiNbO<sub>3</sub> substrate polarization on a charge density at the interface with epitaxial ZnO and Mg<sub>x</sub>Zn<sub>1-x</sub>O films was studied in comparison with ZnO films on dielectric sapphire substrates. An excitonic emission and optical properties such as band gap energy, refraction index, absorption and reflectivity of the ZnO/LiNbO<sub>3</sub> structures were studied. The effect of interface charges on the performance of surface acoustic waves with frequency of 2.7 GHz was investigated, as well. The stimulated cavity mode emission was observed due to attained quasi-phase matching conditions for thin ZnO films on sapphire at high laser excitation power. The positive polarization of the ferroelectric substrate induced the band bending of the semiconductor layer, resulting in the accumulation of the negative charges at the ferroelectric/semiconductor interface, which induced an increased reflectivity, a generation of oxygen emission lines in PL spectra under laser excitation, and an increased electromechanical coupling of surface acoustic waves. The negative polarization of the substrate increased atomic peening during sputtering deposition, which induced deteriorated quality of texture and in-plane orientation and increased the residual stresses in ZnO and Mg<sub>x</sub>Zn<sub>1-x</sub>O films.

**Keywords:** ZnO, LiNbO<sub>3</sub>, polarization, band gap, photoluminescence, surface acoustic waves, interface charges

---

\* samuel.margueron@femto-st.fr

## Introduction

Acoustic-based devices represent the preferred solution for the high-quality factor resonators used in many filtering / sensing technologies. However, telecoms and sensor markets are continuously improving in device performances and functionalities along with increasing the number of active components. The next generations of mobile communication systems will require smart front-end RF signal processing module<sup>1</sup> through the co-integration of acoustic and electronic technologies which address the challenges of frequency agility and dynamical reconfiguration. For instance, a modern signal processing stage should include and combine low noise amplification, complex logical operation of digital/analog signals, agile filtering, switching, acousto-electric mixing, modulation/demodulation, data storage, autocorrelation, time delay, etc. Therefore, the development of tunable acousto-electric devices based on standard acoustic materials such as LiNbO<sub>3</sub> (LN), ZnO, or AlN and semiconductors are of particular interest.<sup>2</sup> However, the coupling of hybrid acoustic/semiconductor technologies will necessitate very sensitive and strong interaction between acoustic and electronic circuitry in a single chip at high frequency.

The interfaces between ferroelectric and semiconductor materials have been studied since early 60s in the frame of development of FeRAMs (ferroelectric random access memory).<sup>3</sup> The induced change of channel conductivity by a factor of  $> 2000$  was demonstrated in the semiconductor SnO<sub>2</sub> deposited on PZT (lead zirconate-titanate) ceramics.<sup>4</sup> Due to electrostatic compensation, negative or positive charges will accumulate in the material in a contact with a polar dielectric depending on its polarity. This effect is enhanced by the energy band distortion. Burfoot and Taylor had explained the role of the band distortion on the accumulation and depletion of the charges at the ferroelectric/semiconductor interfaces.<sup>5</sup> This phenomenon was finally implemented in commercial FeRAM structures based on PZT and CMOS wafers in late 90s. More recently, existence of interfacial charges at ferroelectric–semiconductor capacitors based on PZT/ZnO heterostructures was observed due to band bending.<sup>6</sup> These capacitors were implemented in RLC circuit and a possibility create a controlled shift of resonant frequency with switching ferroelectric polarization was demonstrated. However, PZT layers present high acoustic losses and are not suitable for the high-frequency acoustic wave devices.

The concept of an all-oxide acousto-electronic device was proposed in 2002 by Lu and Emanetoglu<sup>7,8</sup> on r-sapphire. Soon after, in 2004, the formation of two dimensional electron gases (2DEG) in MgZnO/ZnO on sapphire was discovered and patented by Nause and Ganesan.<sup>9</sup> Since then, several groups have published on MgZnO/ZnO 2DEG with a first demonstration of the quantum Hall effect (QHE) in 2008<sup>10</sup> and a mobility of  $10^6$  cm<sup>2</sup>/Vs at 2K<sup>11</sup> obtained. Meanwhile, reports of the performance in frequency at room temperature of MgZnO/ZnO high mobility transistors are almost inexistent. Sasa et al.<sup>12</sup> have shown rather modest results in the GHz range, however, this later paper does not state that 2DEG channel was achieved in their MgZnO/ZnO transistors.

The potential co-integration of semiconductors with LiNbO<sub>3</sub> was first explored by Yi-Yan et al.<sup>13</sup>, Hohkawa et al.<sup>14</sup> and Rotter and al.<sup>15</sup> at the end of the 80's and in the early 90's. Rotter et al. have transferred In<sub>0.2</sub>Ga<sub>0.8</sub>As quantum well containing a 2DEG on LiNbO<sub>3</sub> substrates in order to study the effect of 2DEG on the propagation of surface acoustic waves.<sup>15</sup> The presence of 2DEG on the surface of propagating SAW resulted in the reduced electromechanical coupling, propagation velocity and considerably increased attenuation.<sup>15</sup> The constitutive equation for acoustic waves interaction with 2DEGs was been formalized in 2000 by A. O. Govorov et al.<sup>16</sup> The proof of concept and calculations were based on a delay-line fabricated by transfer and bounding of an InGaAs quantum well. The authors demonstrated the strong interaction of SAW on quantum wells and proposed several original designs in order to study excitonic transition effects<sup>2</sup>. Their technologies were realized by lift-off and transfer of epitaxially grown 2DEGs and other quantum well structures. It yielded rather modest results compared to present filter specifications: losses of less than 3 dB at 2 GHz and above, out-of-band rejection better than 40 dB, etc. (see Campbell<sup>17</sup> for more details about these devices). The performances were limited in frequency by the transfer technique. Since then, there have been a few publications on a Franz-Keldysh acousto-optic modulator<sup>4</sup> and quantized electronic transport by acoustic waves<sup>5</sup>. In the case of acousto-electronic applications, semiconductor/piezoelectric heterostructures are studied not only for the modulation of the acoustic response but also for the transport of charges. A possibility to manipulate the electrical transport in the MoS<sub>2</sub> monolayer by surface acoustic waves excited in LiNbO<sub>3</sub> substrate and the acousto-electric transport in MgO/ZnO-covered graphene were demonstrated very recently by Preciado et al.<sup>18</sup> and Liou et al.<sup>19</sup>, respectively.

Direct epitaxial growth of semiconducting layers enabling a creation of an interfacial charge density in a controlled way on LiNbO<sub>3</sub> (one of the preferred materials for mobile phone RF filters or electro-optic modulators) would facilitate the co-integration of hybrid technology with LiNbO<sub>3</sub> acoustic and optic devices. A possibility to control interface charge density through polarization of a ferroelectric material, which can be reversed locally by applied electric field, would open new opportunities for next generation devices. In this paper, we present a study of the effect of LN substrate polarization on the charge density at the interface with epitaxial ZnO and MgO doped ZnO films. The ZnO films on dielectric sapphire substrates were studied for comparison. An excitonic emission and optical properties such as band gap energy, refraction index, absorption and reflectivity of the ZnO/LiNbO<sub>3</sub> structures were investigated. The effect of interface charges on the performance of high-frequency SAW was observed, as well.

## Experimental details

Epitaxial C-axis oriented (Z-axis oriented) ZnO and Mg<sub>0.22</sub>Zn<sub>0.78</sub>O (MgZnO) films on nonpolar C- (Z-) sapphire and ferroelectric Z-oriented (C-oriented) LiNbO<sub>3</sub> (ZLN) substrates (supplied by Roditi Int. Corp.) were deposited by radio frequency (RF) magnetron sputtering (Plassys MP450S). Films were grown simultaneously on Z+ and Z- polar surfaces of LN substrates (hereafter named as (Z+)LN and (Z-)LN, respectively, while ZLN will be used to describe general cases valid for (Z+)LN and (Z-)LN) during the same run on two pieces cut from the same wafer. For RF sputtering, Zn metal and

Mg<sub>0.22</sub>Zn<sub>0.78</sub>O ceramic targets were used, respectively. ZnO depositions on sapphire substrates were done at temperature of 650 °C and 450 °C, with a power density of 274 mW/cm<sup>2</sup>, a pressure of 2.5 mTorr, and an O<sub>2</sub>/Ar ratio of 1.5. ZnO. Depositions on ZLN were done at lower temperature (450 °C) and with higher power density (548 mW/cm<sup>2</sup>) than those on sapphire substrates in order to avoid chemical interaction between ZnO and LN. MgZnO films were grown at temperature of 400 °C with a power density of 548 mW/cm<sup>2</sup>, a pressure of 6 mTorr, and an O<sub>2</sub>/Ar ratio of 1. The films were etched locally by diluted HCl in order to measure a thickness by a profilometer. The thicknesses of MgZnO films was in the range from 30 nm to 140 nm. ZnO films with thicknesses around 50 nm and 120 nm were deposited on sapphire and ZLN substrates for our study.

Photoluminescence (PL) spectra were collected by using S&I MonoVista Raman spectrometer with excitation of 266 nm. MicroChip laser (TeemPhotonics(TM)) with subnanosecond pulses (0.6 ns) with typical pulse energy of 0.55 μJ and at a repetition rate of 10 kHz was used. Plasma emission was collected with a UV-resistant fiber connected to spectrometer (QE65000, Ocean-Optic) in the range of 300-900 nm. Gallium doped ZnO single crystal (supplied by MTI Corp.) was used as a reference for PL measurements. UVISEL spectroscopic ellipsometer (HORIBA Jobin Yvon) was used to measure ellipsometric spectra from 190 nm (VUV - vacuum ultra violet) to 2100 nm (NIR - near infrared). The ellipsometric data was fitted by using layer/substrate models in order to estimate the absorption, reflectivity and refraction index dependence on the wavelength. It was not possible to use Tauc's method<sup>20</sup> due to the presence of the excitonic peak in the spectra. To fit ellipsometry data and to extract optical properties of the ZnO layers, we have used excitonic model proposed by K. Sato et al.<sup>21</sup> The band gap was evaluated considering a direct transition gap from the photon energy at which the maximum of the absorption occurs. The thicknesses of the films were estimated from ellipsometric data, as well.  $\Theta/2\Theta$  X-ray diffraction (XRD) patterns were collected by using a Bruker D8 Advance diffractometer with monochromatic Cu K $\alpha_1$  radiation (1.54056 Å). The epitaxial quality (rocking curves and  $\phi$ -scans) of the films were measured by using a Bruker D8 Discover diffractometer with Co K $\alpha$  radiation (1.79026 Å). The strain in the films was estimated from the shift of (0002) ZnO reflection in  $\Theta/2\Theta$  X-ray patterns, calibrated with respect to the substrate reflections. The residual stresses were estimated from measured strain values using Hooke's law (elastic constants of ZnO were taken from Hanada et al.<sup>22</sup>). Piezoelectric force microscopy (PFM) was used to map polar domain structure at nanoscale in as-grown ZnO films by using Vertical PFM modes. PFM measurements were done by using NT-MDT NTEGRA system equipped with a Zürich Instrument Dual Frequency Resonance Tracking (DFRT) system. More details concerning PFM measurements and experimental setup can be found in Ref<sup>23</sup>.

Single-port resonators able to excite surface acoustic waves (SAW) with wavelength,  $\lambda$ , of 1.4 μm were designed by freq|n|sys SAS. The single-port resonator consisted of thirty aluminium IDT (interdigital electrodes) pairs and twenty aluminium mirrors on each side of resonator. These resonators were

fabricated by using e-beam lithography (Raith E-line). The fabricated SAW devices were visualized by optical microscopy and scanning electron microscopy (Raith E-line). The thickness of Al electrodes, deposited by evaporation, was 60 nm and additional 200 nm of Al were deposited by RF sputtering on the pads. Two propagation directions,  $\psi$ , in ZnO films were considered according to LN axes: (Z Xt)/0° (X-axis) and (Z Xt)/30° (Y-axis). The resonators were characterized by admittance measurements, using a Vector Network Analyzer (VNA) ROHDE & SCHWARZ. The frequency response was investigated in the range from 2 to 4 GHz. The electromechanical coupling,  $k^2$ , was estimated from the resonance frequency at the maximum of the conductance,  $f_e$ , and the antiresonance frequency at the maximum of the susceptance,  $f_p$ :

$$k^2 = 1 - \left(\frac{f_e}{f_p}\right)^2. \quad (1)$$

Quality factor was estimated from the full width at half maximum (FWHM) of the resonant mode observed in conductance spectrum. Insertion losses were evaluated from the  $S_{12}$  frequency spectra. Current-voltage (I-V) curves in the voltage range from -5 V to 5 V were measured by using dual channel system source meter Kethley 2636b.

## Results

C-axis oriented ZnO films were grown on both C-Sapphire and ZLN substrates (Fig. 1 a). 120-130 nm thick ZnO films on C-sapphire, grown at 650 °C and 450 °C, presented mosaicity of 0.49 ° and 0.69 °, represented by FWHM of (0002) reflection rocking curve (the instrumental contribution was 0.25 °), respectively. The mosaicity of 130 nm ZnO films on (Z+)LN and (Z-)LN substrates was higher (FWHM of 1.28 ° and 2.66 °, respectively) than in case of ZnO/sapphire. The films on both substrates presented single in-plane orientation with respect to the orientation of the substrate, as confirmed by  $\phi$ -scans of ZnO (10 $\bar{1}$ 1) or (11 $\bar{2}$ 2) planes and LN/Sapphire (20 $\bar{2}$ 2) planes. ZnO layers and LN/sapphire substrates presented (10 $\bar{1}$ 0)<sub>ZnO</sub>//(11 $\bar{2}$ 0)<sub>substrate</sub> and (11 $\bar{2}$ 0)<sub>ZnO</sub>//(10 $\bar{1}$ 0)<sub>substrate</sub> epitaxial relationships. In the case of sapphire substrate, misorientations in the plane of 120-130 nm thick films grown at 650 °C and 450 °C were around 1.05 ° and 1.23 ° (represented by FWHM of (10 $\bar{1}$ 1) reflections in  $\phi$ -scans, instrumental resolution was 0.38° for these measurements), respectively. Disorder in the substrate plane was considerably higher in 130 nm thick ZnO films on (Z-)LN films (FWHM=3.80 ° of (1122) reflections in  $\phi$ -scans) and ZnO/(Z+)LN (FWHM= 2.24 °) substrates than in the films on sapphire substrates. It is important to note that the mosaicity and the orientation in the substrate plane were more disordered in the case of (Z-)LN substrates than on (Z+)LN. In the case of 50 nm thick ZnO films, the difference in quality of texture and in-plane orientation between films grown on (Z+) and (Z-) LN substrates was less pronounced: (i) FWHMs of (0002) rocking curves were 2.52 ° and 2.75 °, (ii) FWHMs of (11 $\bar{2}$ 2) reflections in  $\phi$ -scans were 2.82 ° and 2.78 °, respectively. MgZnO layers on LN substrates showed similar texture and epitaxial quality to that of ZnO/ZLN films. 140 nm (50 nm) thick MgZnO

films on (Z+) and (Z-) presented mosaicity of 1.45 ° and 1.90 ° (1.40 ° and 2.11 °) and misorientation in-plane of 2.24 ° and 2.59 ° (2.03 ° and 2.78 °), respectively. The difference in structural quality on substrates with opposite polarization direction was identified in MgZnO films, as well.

The shift of ZnO reflections towards lower  $2\theta$  angles in XRD  $\theta/2\theta$  patterns indicated an elongation of C-lattice parameter and biaxial compressive strain in the substrate plane (Fig. 1). 50 nm thick ZnO films on sapphire deposited at 450 °C and 650 °C, were under -0.6 GPa and -0.4 GPa (with error of  $\pm 0.1$  GPa) in-plane stress, respectively. In the C-ZnO on ZLN substrates, the residual stress state was dependent on the substrate polarity. The compressive residual stresses of -1 GPa and -0.6 GPa were present in 130 nm thick ZnO films and they were of -0.5 GPa and -0.3 GPa in 50 nm thick films on (Z-) and (Z+) LN substrates, respectively. C-ZnO presented larger in-plane lattice parameters than ZLN and C-sapphire. Therefore, ZnO films grew under compressive misfit strain of 8.4% and 18.2% (in-plane mismatch of unit cells), respectively. In order to match on C-sapphire and ZLN, 11 unit cells of C-ZnO are placed on the 13 cells of C-sapphire and 12 cells of ZLN by reducing the mismatch to 0.03 % and 0.07 %, respectively. This would result in compressive misfit stress of -0.07 GPa and -0.16 GPa, if the relaxation by misfit dislocations at the film-substrate interface were not present. The lattice misfit stress is usually relaxed in the first tens of nm of epitaxial films on not perfectly matching substrate.<sup>24,25</sup> C-ZnO presents very similar in-plane thermal expansion coefficient ( $4.3 \times 10^{-6} \text{ K}^{-1}$ ) to that of C-sapphire ( $4.5 \times 10^{-6} \text{ K}^{-1}$ ) and several times smaller than that of ZLN ( $19.2 \times 10^{-6} \text{ K}^{-1}$ ).<sup>26</sup> Therefore, the thermal stress was small in the case of C-ZnO/C-sapphire structure (-0.010 GPa and -0.015 GPa in films grown at 450 °C and 650 °C, respectively) and C-ZnO films on ZLN was under higher compressive thermal stress (-0.77 GPa). Thus, the experimentally measured residual stresses of -(0.4-0.6) GPa in ZnO films on sapphire substrates could not originate just from misfit and thermal stresses. This indicated that compressive intrinsic stresses, generated by the atomic peening during deposition by sputtering technique, were dominating in our films. It was also reported -(0.33-0.55) GPa compressive residual stresses in ZnO/sapphire films grown by pulsed laser deposition and it was concluded that these residual stresses were defined by the plasma bombardment conditions.<sup>27</sup> The increase of residual stresses in thicker ZnO films on LN substrates, confirmed this hypothesis.

It was not possible to estimate the residual stresses in MgZnO films from lattice parameters due to the presence of composition effect. However, the 130 nm thick ZnO films on LN substrates presented higher stresses than 50 nm thick films and higher residual stresses were accumulated in the case of (Z-)LN substrates than in films on (Z+)LN substrates. Thus, one could expect the increase of stresses with the increase of the thickness of MgZnO films and on (Z-)LN substrates, as well. Unfortunately, it was not possible to compare the residual stress values in MgZnO and ZnO films.

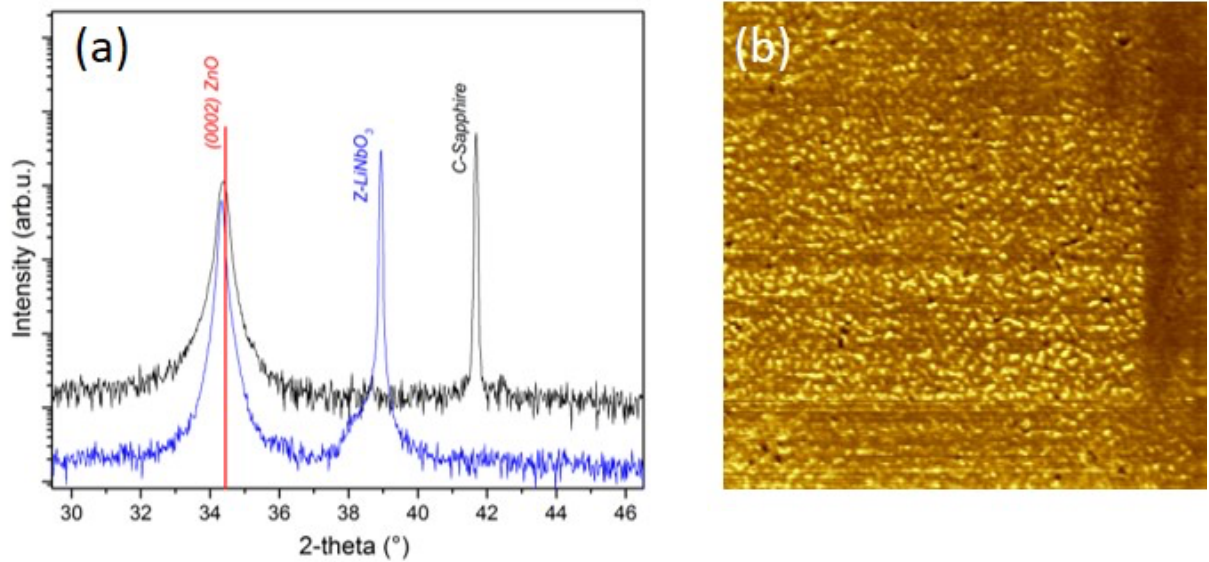


Fig. 1  $\Theta/2\Theta$  X-ray diffraction patterns of ZnO films on sapphire and LN substrates (a). PFM amplitude image ( $2 \mu\text{m} \times 2 \mu\text{m}$ ) of ZnO layer on (Z-) LN substrate (b).

MgZnO and ZnO films were grown on both (Z-) and (Z+) LN substrate surfaces. It is expected that ZnO films, grown by sputtering techniques at high oxygen partial pressure, present oxygen terminated surface and negative polarity.<sup>28</sup> ZnO on dielectric sapphire substrates presented oxygen termination independently of applied bias voltage.<sup>29</sup> In our case, the polarity of ZnO films could be moreover altered by the spontaneous polarization of (Z-)/(Z+) LN and/or charges present on the ferroelectric substrate surface, generated by strain, pyroelectricity or ferroelectric/semiconductor junction. In order to check if there was a difference in a ZnO growth rate on (Z+) and (Z-) LN surfaces, the film thicknesses of ZnO films grown on these surfaces during the same run were estimated by means of ellipsometry. Two runs were compared, in order to evaluate the reproducibility and homogeneity. During the first run, the thicknesses of films on (Z+) and (Z-) surfaces were 124 nm and 128 nm, respectively. During the second run, the film on (Z+) LN was thicker by 9 nm than on (Z-) surface. This indicates that the differences in measured thicknesses are related to the errors of the thickness measurements ( $\pm 5$  nm) and homogeneity of the deposition. In the case of sputtering technique, growth rates are little dependent on the substrate and substrate temperature and are mainly defined by plasma conditions. We were not able to identify the sign of ZnO polarity by pyroelectric current measurements, as well. The measured pyroelectric current followed the current generated by LN, as LN had much higher pyroelectric coefficients than ZnO. According to PFM measurements, grown ZnO films presented homogenous polarity (Fig. 1 b). However, PFM technique was not able to determine the difference in polarity sign on two different samples. At this stage of our study, the polarity signs of MgZnO and ZnO films remained unknown.

LN presents an indirect bandgap, which energy varies from 3.6 eV to 3.8 eV. In literature, it was reported that the energy gap shifted towards higher energy in ZnO films doped by MgO.<sup>30</sup> 14 mol%

MgO doping was necessary to attain bandgap higher than 3.6 eV.<sup>30</sup> In order to obtain ZnO films with lower and higher bandgap as compared to LN, pure ZnO and MgZnO (using target MgZnO with 22 mol% of MgO) films were grown. The estimation of MgO concentration in grown MgZnO films from lattice parameters, as proposed by Ashrafi et al.,<sup>31</sup> was not straightforward, due to the presence of high residual stresses. Therefore, we have made an assumption that residual stresses in MgZnO/sapphire films are comparable (-0.6 GPa) to those in ZnO/sapphire films, as mainly intrinsic stresses were dominating in the case of sapphire substrates. The c-lattice parameters of MgZnO/sapphire films were compared to those of ZnO/sapphire films, grown also by sputtering technique, in order to take into account the residual stress effect and to estimate the MgO concentration using Ashrafi et al. calibration. The MgO concentration within the grown MgZnO films was estimated to be around 17.6 mol%. Ashrafi et al. have achieved the precision of  $\pm 3$  mol% by using this method. However, in our case, the precision might be around 5 mol% as the plasma conditions were not identical in the case of ZnO and MgZnO films. This would suggest that MgZnO films contained similar or lower MgO composition than used MgZnO target.

The absorption spectra (obtained from ellipsometric measurements) of MgZnO/(Z+)LN and ZnO films on sapphire, (Z+)LN and (Z-)LN substrates in comparison to absorption of Ga:ZnO single crystal with negative surface polarity are represented in Fig. 2 a. The bandgaps of ZnO films on (Z+) and (Z-)LN substrates were almost identical (3.36 eV and 3.35 eV, precision of ellipsometric method was of  $\pm 0.02$  eV) and very close to that of Ga:ZnO single crystal (3.33 eV). ZnO/sapphire films presented bandgap of 3.31 eV. In the case of MgZnO films, reliable fitting of the ellipsometry data could be attained only for films on (Z+)LN substrates. The estimated bandgap of MgZnO films was 3.79 eV, which was considerably higher than that of ZnO films (Fig. 2 a). According to the relationship between the bandgap and MgO composition in  $Mg_xZn_{1-x}O$  films, reported by Ohtomo et al.<sup>30</sup>, the bandgap of 3.79 eV corresponds to the MgO composition of 21.9 mol%. This confirmed that our sputtered MgZnO film composition was similar to that of the target. The refraction index and reflectivity as a function of wavelength were estimated by means of ellipsometry, as well. At high wavelengths ( $> 450$  nm), experimentally estimated refraction index of 54 nm ZnO/Sapphire films was very close to that of Ga-doped ZnO crystal. Our measurements were also in a good agreement with literature data<sup>32</sup> (Fig. 3 a). At the wavelengths close to the energy of the band gap, refraction index was highly dispersive and deviated from that of bulk ZnO due to difference in the energy of band gap of two materials (Fig. 3 a). The reflectivity of ZnO films on LN substrates was highly sensitive to the direction of the spontaneous polarization of the substrate (Fig. 2 b). The reflectivity of ZnO films on (Z-) LN substrates was considerably lower than that of equivalent films on (Z+) LN substrates. The possible origins of the increased reflectivity might be surface roughness and structural defects. However, ZnO films on (Z-)LN was considerably rougher (roughness RMS was 3.6 nm) when ZnO/(Z+)LN films (RMS=1.7 nm). As mentioned above, the texture quality of ZnO/(Z-)LN films was worse as compared to that of

ZnO/(Z+)LN, as well. Thus, the increased reflectivity of ZnO/(Z+)LN films cannot be attributed to the structural and surface defects.

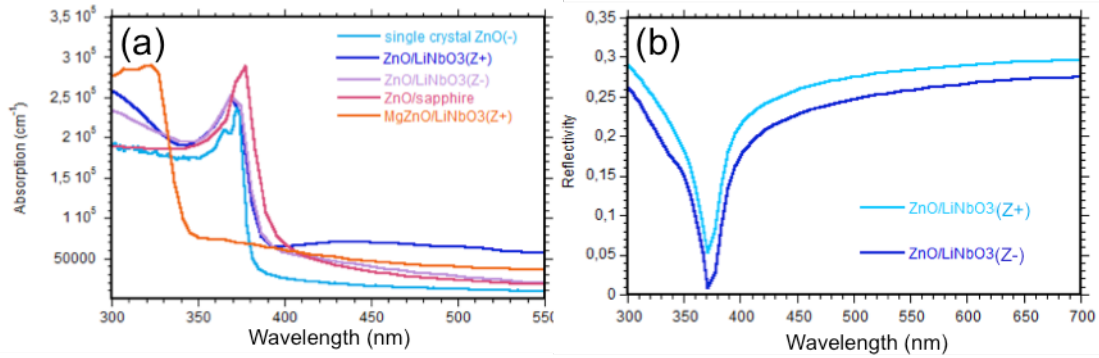


Fig. 2 Absorption as a function of wavelength of MgZnO/(Z+)LN and ZnO films on sapphire, (Z+)LN and (Z-)LN substrates in comparison to absorption of Ga:ZnO single crystal with negative surface polarity (a). Reflectivity change as a function of wavelength of 115 nm thick ZnO films on (Z+) and (Z-) LN substrates (b).

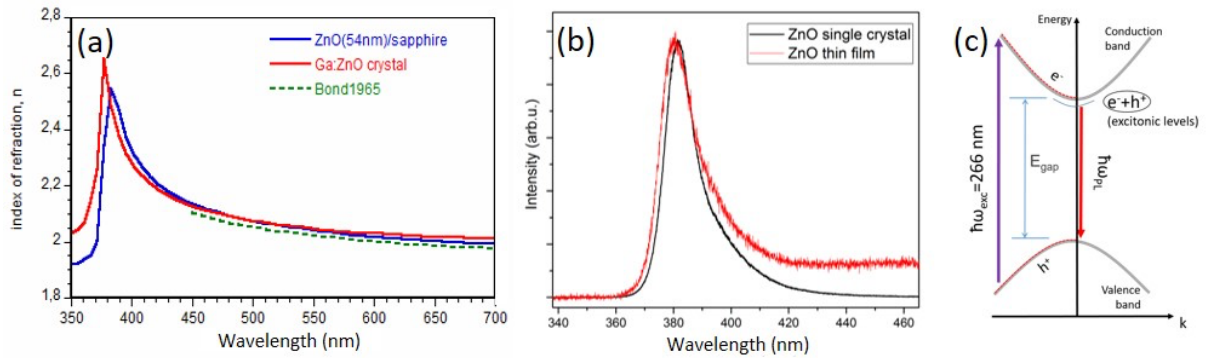


Fig. 3 Comparison of wavelength dispersions of refraction index, estimated by means of ellipsometry (a) and excitonic emission in PL spectra (b) of 54 nm thick ZnO film on sapphire, Ga doped ZnO single crystal and literature data<sup>32</sup>. Schematic representation of the PL phenomenon, energy gap and excitonic levels (c).  $E_{gap}$  stands for band gap energy,  $k$  – wavenumber,  $e^-$  – electrons,  $h^+$  – holes,  $\hbar\omega_{exc}$  – laser excitation energy,  $\hbar\omega_{PL}$  – PL energy.

The electronic structure of ZnO based materials was studied by using photoluminescence spectroscopy. PL spectrum of 54 nm thick ZnO film on C-sapphire is given in Fig. 3 b. PL peak observed at 380.6 nm (Fig. 3 b) corresponded to the emission of free excitonic levels near band gap (380.3 nm) in direct semiconductor, observed due to photoexcitation of electrons in the conduction band by laser (Fig. 3 c). The blue shift of excitonic level in ZnO film as compared to that of ZnO single crystal (381.6 nm) confirmed the presence of compressive stress in epitaxial ZnO films on sapphire substrate (Fig. 3 b). In the case of thin film, an additional luminescence was present at longer wavelengths ( $> 390$  nm) which represented other luminescence defects at lower energy levels within the band gap. Moreover, PL spectra measured at room temperature were dependent on the laser excitation intensity. In order to illustrate this phenomenon, PL spectra were collected as a function of a distance of a laser focus (Z-

scan, given in Fig. 4 a). The Z-scan was realized by approaching the focal point of the laser with power of 1 mW from height of 500  $\mu\text{m}$  to the sample surface by steps of 50  $\mu\text{m}$ . The maximum power was attained when the focal point was on the sample surface. The intensity of exciton emission increased by increasing the excitation intensity. At a certain point, stimulated emission occurred in parallel to the exciton emission, represented by fine emission peaks at wavelengths corresponding to the cavity modes. The exciton emission totally disappeared and only cavity modes were observed at the maximum power of excitation (Fig. 4 b). The wavenumbers of observed cavity modes were highly dependent on the location in the sample. These cavity modes satisfied the quasi phase matching condition<sup>33</sup>:

$$m = \frac{2Ln}{\lambda_0}, \quad (2)$$

Where  $m$  is a number of half-wavelengths in the length of resonant cavity,  $L$ , representing resonant mode harmonics,  $n$  is a refractive index of the layer, and  $\lambda_0$  – a wavelength of exciton emission. In the case of ZnO/sapphire layer, the length of resonant cavity was represented by the thickness of ZnO layer (54 nm). Thus, even small variations in the film thickness ( $L$ ) would affect the quasi phase matching conditions. The exciton emission was represented by the dispersion in the wavelength range from 375 nm to 400 nm. In this wavelength range, the refractive index of ZnO layer ( $n$ ) was highly dispersive, as well. It varied from 2.4 to 2.2, respectively. Dispersive behaviour of refractive index and exciton emission resulted in a multiplicity of observed cavity modes. Moreover, the positioning of focal point at the different places in the sample was not exactly identical (due to the imprecision in the focus), and therefore the satisfaction of quasi phase matching conditions ( $m$ ) was changing and consequently the observed cavity modes were different, as well.

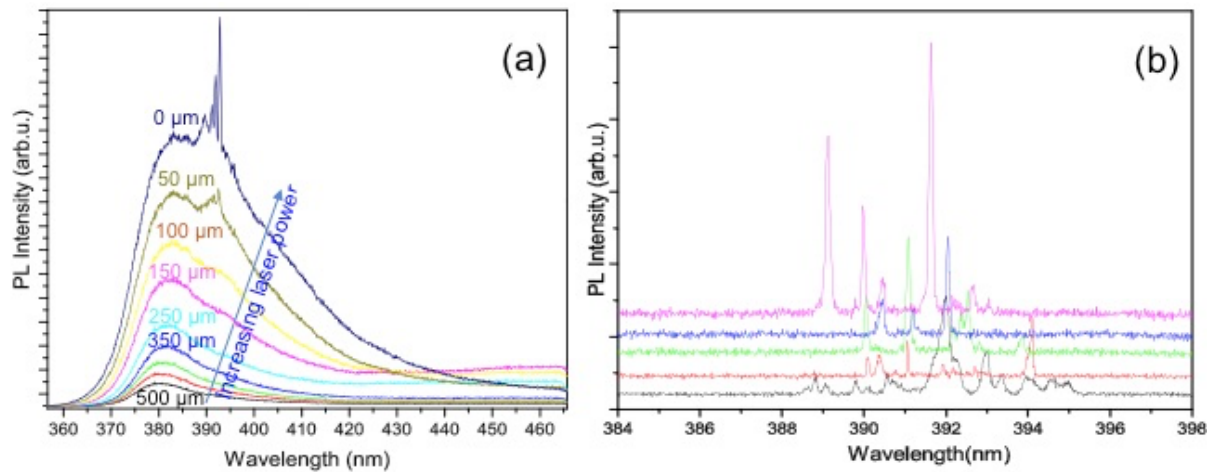


Fig. 4 Excitonic emission in PL spectra of 54 nm thick ZnO film on sapphire as a function of laser power. The power of the laser was tuned by approaching the focal point of the objective from height of 500  $\mu\text{m}$  to sample surface, height of 0  $\mu\text{m}$  (a). The spectra of cavity modes, observed in different places of the sample at high laser pumping field (b).

PL spectra of ZnO and MgZnO films on (Z-) and (Z+) LN substrates are compared in Fig. 5. In the case of (Z-) LN substrates, only emission of excitonic levels was observed. The excitonic emission at 379.3 nm of ZnO/(Z-)LN films was observed at lower wavelengths than those of ZnO/sapphire films and ZnO single crystal. The ZnO/(Z-)LN films have presented higher compressive stresses (1 GPa) with respect to those in ZnO/sapphire films (0.4 GPa) and ZnO single crystal (stress-free). Thus, the observed difference in the exciton emission at least partially might be related to the difference in a stress state in the films. Lower wavelengths of exciton emission of MgZnO films are expected due to higher energy of band gap of these films. The absorption of UV wavelengths by optical components of spectrometer did not allow measuring the complete profile of excitonic emission and in the case of MgZnO films, the maximum of excitonic emission could not be observed. Nevertheless, it clearly can be seen that the excitonic emission of MgZnO films presented a maximum emission at lower wavelengths to those ZnO films (Fig. 5). The PL spectra of films on (Z+) LN substrates showed totally different features (Fig. 5). Fleeting emission of the spectrum, represented by typical emission lines of oxygen, was observed. The attribution of these emission lines was done in comparison with LIBS (laser-induced breakdown spectroscopy) spectra.<sup>34</sup> It should be pointed out that no Zn emission lines were observed which indicated Zn ions were not ablated by laser.<sup>35</sup> In this case, exciton emission was difficult to detect due to the small integration time (< 1 s) (Fig. 5). This phenomenon was observed only for ZnO and MgZnO films grown on (Z+) LN polarity substrates. This emission was very short in duration and occurred during the first fractions of a second after switching on the laser. After this short duration, this emission, lines disappeared and the excitonic emission with too low intensity for analysis was observed..

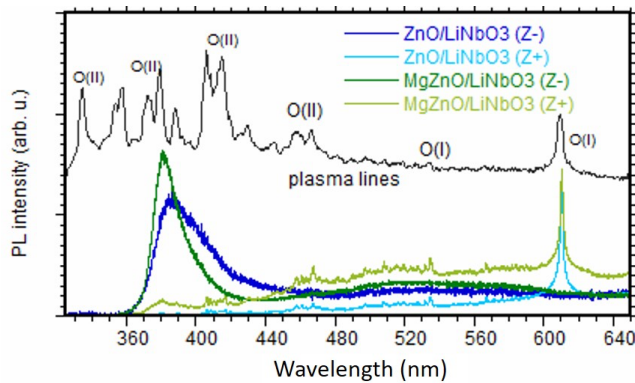


Fig. 5 PL spectra of 115 nm ZnO and 30 nm MgZnO films on (Z+) and (Z-) LN substrates. The absorption of UV wavelengths (< 370 nm) by optical components of spectrometer did not allow to measure the complete profile of excitonic emission. Emission spectrum of oxygen plasma lines is given for comparison.

In this study, the effect of LN substrate polarity on a charge density at ZnO/LN interface was studied. I-V curves and estimated conductivity values of 120 nm thick ZnO and MgZnO films on (Z+)LN and (Z-)LN substrates are represented in the Fig. 6. The conductivity of all ZnO and MgZnO layers was residual as these materials were undoped semiconductors. The ZnO and MgZnO films on (Z-)LN substrates presented the conductivity below  $10^{-10}$  S. The conductivity was considerably higher in ZnO

and MgZnO films grown on (Z+) LN substrates ( $4.2 \times 10^{-8}$  S and  $3.6 \times 10^{-9}$  S, respectively) as compared to films on (Z-)LN substrates.

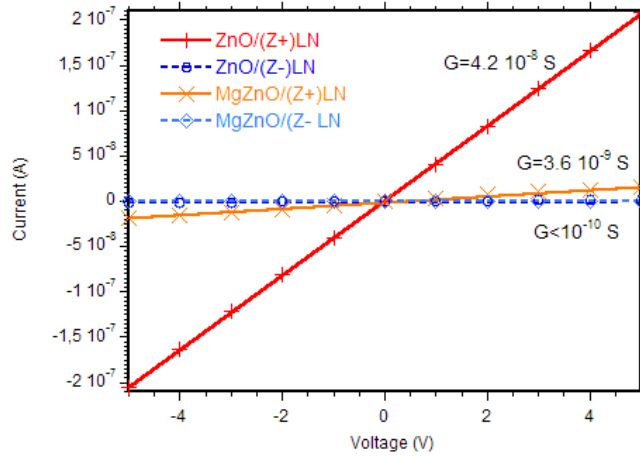


Fig. 6 I-V curves of ZnO and MgZnO films on (Z+)LN and (Z-)LN substrates ( $G$  represents conductivity,  $I$  – current, and  $V$  – voltage).

Single-port SAW resonators with wavelength of  $1.4 \mu\text{m}$  were fabricated on the  $115 \text{ nm}$  thick ZnO films on the (Z-) and (Z+) LN substrates (Fig. 7). SAW propagation along Y ( $0^\circ$ ) and X ( $30^\circ$ ) LN axes was studied in the case of ZnO/(Z-)LN. It is important to note that X (Y)-axis of ZnO was parallel to Y(X)-axis of LN. In the case of both propagation directions, the insertion losses were low (2.4-2.5 dB). Single SAW resonant mode at 2.70 GHz and 2.80 GHz was observed in the 2 – 4 GHz frequency range, representing 3780 m/s and 3920 m/s propagation velocities along Y- and X-axis of (Z-) LN, respectively (Fig. 8 a). The velocity of Rayleigh wave in Z-cut LN single crystal is much higher (3840 m/s along X-axis) than in ZnO (2700 m/s).<sup>36</sup> Therefore, the SAW was guided by ZnO layer and presented dispersive properties. The acoustic energy was mainly located in the LN substrate surface as ZnO layer thickness is much lower than the SAW wavelength. Therefore, SAW properties are mainly defined by the elastic properties of LN substrate. The  $k^2$  of Rayleigh modes, propagating along X- and Y-axis, were 0.94 % and 0.36 % (the quality factors were 491 and 455), respectively. In the case of ZnO films on (Z+) LN substrates, only SAW propagating along LN Y-axis was studied. In the case ZnO/(Z+)LN, insertion losses were slightly higher (3.3 dB). The main resonant mode was observed at 2.73 GHz and the secondary mode at 2.71 GHz (Fig. 8 a). The mode at 2.71 GHz presented similar  $S_{11}$  signal intensity to that of resonant mode at 2.70 GHz in ZnO/(Z-)LN. The  $k^2$  of modes at 2.71 GHz and 2.73 GHz were 0.68 % and 0.89 % (Fig. 8 b), respectively. The electromechanical coupling was several times increased in the case of ZnO films on LN substrates with positive polarization direction as compared to that on (Z-) LN substrates. The higher  $k^2$  was confirmed also by the increased conductance values of resonant modes (Fig. 8 b). Higher electromechanical coupling resulted in the decrease of the quality factor (250) in ZnO/(Z+)LN structure.

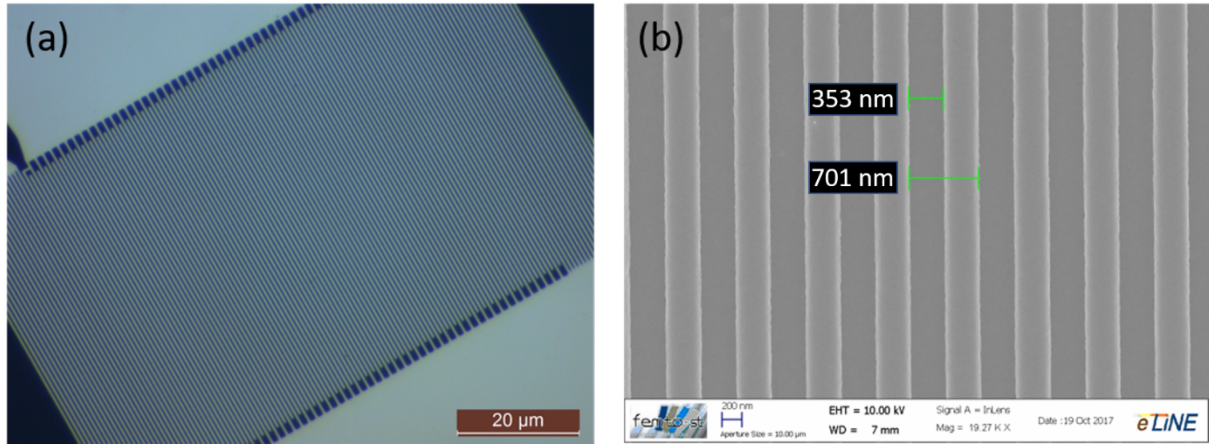


Fig. 7 Optical (a) and SEM (b) images of SAW resonator with wavelength of  $1.4 \mu\text{m}$ .

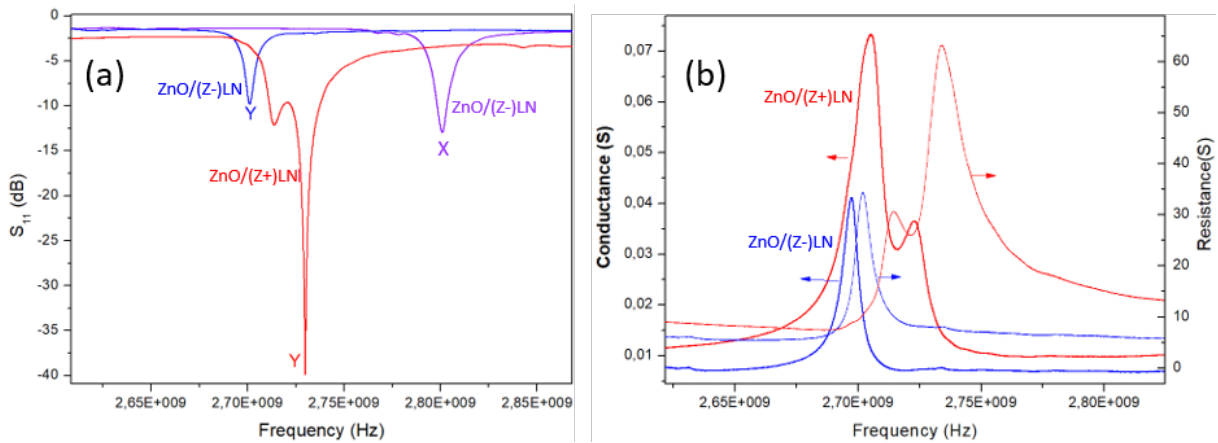


Fig. 8 Power reflection coefficient,  $S_{11}$ , (a) conductance and resistance (b) of Rayleigh mode with wavelength of  $1.4 \mu\text{m}$  propagating along Y and X-axes of LN in ZnO/(Z+)LN and ZnO/(Z-)LN heterostructures.

## Discussion

In the case of ZnO films on non-polar and non-ferroelectric dielectric substrates such as sapphire, PL spectra presented the emission of free excitonic levels close to the bandgap energy. The excitons did not dissociate on the film surface which indicated that excitons could be confined inside the layer thickness. Moreover, at low thickness of ZnO layer and high laser pumping field, quasi-phase matching conditions were achieved for exciton emission wavelength and cavity modes were observed. The lifetime of the excitons was long enough for stimulated emission<sup>37</sup> in the cavity. The ZnO and MgZnO films grown on (Z-)LN substrates presented considerably higher compressive stresses than films on (Z+)LN substrates, due to electrostatic attraction of  $\text{Ar}^+$  ions and consequently increased atomic peening during sputtering deposition, which induced deteriorated quality of texture and in-plane orientation. In the cases of (Mg)ZnO films, the distortion of energy bands occurred at the LN and (Mg)ZnO interface due to polarisation state of LN (Fig. 9). This explains, the accumulation of charges in the case of MgZnO and ZnO films on (Z+) LN substrates as indicated by conductivity measurements. It is important to note

that the polarity of the substrate did not affect the energy itself of the bandgap of ZnO films. The band bending in the semiconductor results in the accumulation or depletion of charges due to ferroelectric polarization, which has been observed for ferroelectric memories (FeRam).<sup>3,4,5</sup> According to Gauss theorem, the accumulated charge density at the ZnO side of the interface ZnO/substrate,  $\rho$ , depends on a total polarization of the heterostructure,  $\Delta P_{tot}$ :

$$\rho = -div \Delta P_{tot}. \quad (3)$$

$\Delta P_{tot}$  depends not only on the spontaneous polarization,  $P_s$ , of the film,  $P_{s(ZnO)}$ , and the substrate,  $P_{s(LN)}$ , but also on the induced polarization by present stresses,  $P_{ind}$ <sup>38</sup>:

$$\Delta P_{tot} = \pm P_{s(ZnO)} \pm P_{s(LN)} - P_{ind}, \quad (4)$$

$$\text{and } P_{ind} = \left( e_{31} - e_{33} \frac{c_{31}}{c_{33}} \right) (\varepsilon_1 + \varepsilon_2), \quad (5)$$

Where  $\varepsilon_i$  is a deformation,  $e_{ij}$  and  $c_{ij}$  are piezoelectric and compliance constants of the ZnO film, respectively. In the case of 120 nm thick ZnO films on (Z-) and (Z+) LN substrates,  $P_{ind}$  were of 0.016 C/m<sup>2</sup> and 0.009 C/m<sup>2</sup> (estimated from experimentally measured strain values, elastic and piezoelectric constants were taken from Ref. 22), respectively. The  $P_{s(ZnO)}$  and  $P_{s(LN)}$  were - 0.057 C/m<sup>2</sup><sup>22</sup> and 0.75 C/m<sup>2</sup>, respectively. Although, the spontaneous polarization of LN substrate is dominating, the contribution of residual stresses to the polarization of ZnO layers is considerable. Moreover, the compressive residual stresses would increase the spontaneous polarization of ZnO films with negative polarity. In the case of ZnO/(Z-)LN structure, electrons did not cumulate at the interface between LN and ZnO due to negatively charged LN surface. When the surface polarization of LiNbO<sub>3</sub> was Z+, the accumulation of positive charges in the surface layer of LN tended to increase an electron density at the ZnO side of the ZnO/LiNbO<sub>3</sub> interface. This presence of interface charges could induce the increased reflectivity and could make the surface of ZnO poor in electrons, which weakened the Zn-O bondings on the surface and facilitated the ablation of surface atoms by laser light and their emission lines visible in the PL spectra of (Mg)ZnO/ (Z+)LN, while standard emission of excitons was visible in PL spectra of (Mg)ZnO/(Z-)LN (similar to that on dielectric substrates). Oxygen emission lines were observed in PL spectra of both ZnO and MgZnO films on (Z+) LN substrates. Although, we were not able to determine polarity of (Mg)ZnO films, the absence of Zn emission lines and ablation of oxygen atoms might indicate that the ZnO and MgZnO surface on (Z+)LN substrates had oxygen-termination (negative polarity). In order to generate sheet conductivity at the interface, a layer has to present bandgap energy higher than a substrate. However, the ZnO layer contained lower bandgap than LN. In the case of MgZnO films, generation of 2DEG could be possible but it was not studied in our case. The emission of excitonic levels and its dispersion depends on the film thickness/ stress state, present defects and doping level. It was reported that the thickness of ZnO in which the charges are cumulated was around 27 nm<sup>39</sup>. However, the generated plasma lines were comparable for 30 nm thick MgZnO films and 115

nm thick ZnO films. This indicated that the interface charges could be generated mainly due to positive polarization of the substrate independently of the difference in the film/substrate bandgaps, film thickness and stress state in agreement with the dominating contribution of  $P_{s(LN)}$  in Eq. 4 and 3.

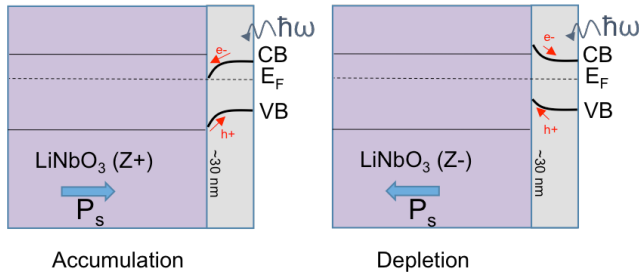


Fig. 9 Schematical representation of the energy band distortion of the semiconductor (Mg)ZnO layer with alignment of Fermi level at the interface with ferroelectric (Z+) and (Z-) LN substrate. The bending of LN energy bands was not represented.  $E_C$  stands for conduction band energy,  $E_F$  - Fermi level energy,  $E_V$  - valence band energy,  $e^-$  - electrons,  $h^+$  - holes,  $\hbar\omega_{exc}$  - laser excitation energy. Blue arrow indicates the ferroelectric polarization direction of LN.

In the literature, the theoretical analysis of acoustical parameters showed that a big difference was expected in electromechanical coupling in the case of ZnO films on positive and negative surface of ZnO/128°-rotated Y-cut LN.<sup>40</sup> Higher  $k^2$  was simulated and measured in X-ZnO films with polarization axis in the substrate plane on positive surface than on negative surface of (01 $\bar{1}2$ ) LiTaO<sub>3</sub> substrates.<sup>41</sup> However, the agreement between simulation and experimental results was not good. It is important to note that a distortion of energy band and an accumulation/depletion of charges were not taken into account in these studies. In both cases, LN and LiTaO<sub>3</sub> substrates were studied with oblique orientations of polar axis thus, the angle of polar axis with surface normal was different on positive and negative surfaces of LN and consequently the acoustical properties were not identical for both surfaces as shown by these two literature reports.<sup>40,41</sup> In our case, we expect identical acoustical performance on (Z+) and (Z-) LN surfaces, although it still needs to be proven by simulations once the polarity sign of ZnO films will be identified.

The evidence that presence of free charges induce a change in frequency of SAW devices was shown by a photo-generation (UV light) of carriers in semiconducting ZnO layers on LN substrates.<sup>42</sup> In this work, the accumulation of the negative charges at the film/substrate interface induced the increased reflectivity of ZnO/(Z+)LN films and highly affected the SAW generation. SAW, excited by the top interdigital metal electrodes (IDTs), propagated together with its potential inducing the periodic distribution of free charges at the ZnO/(Z+)LN interface. These interface charges contributed additionally to the efficiency of the SAW wave excitation, which resulted in the considerably ameliorated electromechanical coupling of waves. The double resonance mode can be related to the shift

of the main SAW resonance to the higher/lower frequencies due to the several possible origins: (i) additional SAW excitation with electrodes without mass (or mass corresponding to the 27 nm of ZnO with free carriers); (ii) difference in periodicity of the charge distribution at the interface and IDTs; (iii) difference in excitation (efficiency and velocity) by charges located on the ZnO film surface and at the ZnO/LN interface. The imprecision in propagation angle was  $\pm 5^\circ$ , which would correspond to the shift of mode frequency by 0.017 GHz. Thus, it was not evident to distinguish which mode was the main one, excited by the interdigital electrodes and which was due to interfacial charges. One could expect that the better coupled mode at 2.73 GHz should be excited by the charges at the interface with LN. However, further theoretical and experimental studies are needed in order to understand the relationship between presence of the interface charges and the SAW performance.

### Concluding remarks

Epitaxial C-axis oriented ZnO and MgZnO films with homogeneous polarity on C-sapphire and (Z-) and (Z+) LN substrates were studied by means of photoluminescence spectroscopy and ellipsometry. The excitonic emission was observed in PL spectra of ZnO films on dielectric sapphire and ferroelectric (Z-) LN substrates. The stimulated cavity mode emission was observed due to attained quasi-phase matching conditions for 54 nm thick ZnO films at high laser power. The excitonic emission, energy band gap and the related properties of the ZnO films were slightly affected by the residual stresses. In order to attain the higher band gap (3.8 eV) of ZnO films than that of LN, ZnO films were doped by 22 mol% of MgO. It was proven, that the presence of polar substrate affected the structural, optical and photoluminescence properties of semiconductor film. The negative polarization of the LN substrate increased atomic peening during sputtering deposition, which induced deteriorated quality of texture and in-plane orientation and increased the residual stresses in ZnO and MgZnO films. Both ZnO and MgZnO films on (Z+) LN substrates presented considerably different properties such as increased reflectivity and conductivity, generation of oxygen emission lines in PL spectra under laser excitation, and increased electromechanical coupling of SAW resonators as compared to the films on (Z-) LN and sapphire substrates. The bandgap energy was not affected by the substrate polarity. The positive polarization of the ferroelectric substrate induced the band distortion of the semiconductor layer, resulting in the accumulation of the negative charges at the ferroelectric/semiconductor interface. The presence of charges affected optical properties such as reflectivity of film and the excitation of the surface acoustic waves (electromechanical coupling, losses and frequency). Although, further studies are needed of this phenomenon, these preliminary results clearly indicated new unexplored possibilities for the optical/acoustical applications of ZnO and LN.

## Acknowledgments:

This work was supported by the French RENATECH network, Labex First-TF (contract No. ANR-10-LABX-48-01), EUR EIPHI program (contract No. ANR-17-EURE-0002) and French National Research Agency fundings ANR LiLit (contract No. ANR-16-CE24-0022-011). The authors also thank the BQR ENSMM for financial support through the IFE project.

## References

- 
- <sup>1</sup> P. Choi, S. Goswami, U. Radhakrishna, D. Khanna, C.-C. Boon, H.-S. Lee, D. Antoniadis, and L.-S. Peh, *IEEE Trans. Microw. Theory Techn* 63 (4), 1163 (2015).
  - <sup>2</sup> A. Bartasyte, S. Margueron, T. Baron, S. Oliveri, and P. Boulet, *Adv. Mater. Interfaces* 1600998 (2017).
  - <sup>3</sup> J. L. Moll and Y. Tarui, *IEEE Trans. Elec. Dev.* 10 (5), 338 (1963).
  - <sup>4</sup> J. C. Crawford and F.L English, *IEEE Trans. Elec. Dev.* 16 (6), 525 (1969).
  - <sup>5</sup> J. C. Burfoot and G. W. Taylor, *Polar dielectrics and their applications*, University of California Press (1979).
  - <sup>6</sup> E. Cagin, D. Y. Chen, J. J. Siddiqui, and J. D. Phillips, *J. Phys. D: Appl. Phys.* 40, 2430 (2007).
  - <sup>7</sup> Y. Lu and N. W. Emanetoglu, US patent US20020044028 A1 (2002).
  - <sup>8</sup> N. W. Emanetoglu, J. Zhu, Y. Chen, J. Zhong, Y. Chen, and Y. Lu, *Appl. Phys. Lett.*, 85, 3702 (2004).
  - <sup>9</sup> J. Nause and S. Ganesan, US patent 2004/0056273A1 (2004).
  - <sup>10</sup> A. Tsukazaki, H. Yuji, S. Akasaka, K. Tamura, K. Nakahara, T. Tanabe, H. Takasu, A. Ohtomo, and M. Kawasaki. *Appl. Phys. Express*, 1, 055004 (2008).
  - <sup>11</sup> J. Falson, Y. Kozuka, M. Uchida, J. H. Smet, T. Arima, A. Tsukazaki, and M. Kawasaki, *Scientific Reports* 6, 26598 (2016).
  - <sup>12</sup> S.Sasa, T. Maitani, Y. Furuya, T. Amano, K. Koike, M. Yano, and M. Inoue, *Phys. Status Solidi A* 208 (2), 449 (2011).
  - <sup>13</sup> A. Yi-Yan, W.K. Chan, T.J. Gmitter, L.T. Florez, J.L. Jackel, E. Yablonovitch, R. Bhat, and J.P. Harbison, *IEEE Photon Technol. Lett.* 1, 11 (1989).
  - <sup>14</sup> K. Hohkawa, H. Suzuki, Q.S. Huang, and S. Noge, *IEEE Ultrason. Symp.*, 401 (1995).
  - <sup>15</sup> M. Rotter, W. Ruile, G. Scholl, and A. Wixforth, *IEEE Trans. Ultrason., Ferroelect., Freq. Control* 47, 242 (2000).
  - <sup>16</sup> A.O. Govorov, A.V. Kalameitsev, M. Rotter, A. Wixforth, J.P. Kotthaus, K.-H. Hoffmann, and N. Botkin, *Phys. Rev. B* 62, 2659 (2000).
  - <sup>17</sup> C. Campbell, *Surface Acoustic Wave Devices and Their Signal Processing Applications*, Academic Press Inc. (1989).
  - <sup>18</sup> E. Preciado, F. J.R. Schulein, A. E. Nguyen, D. Barroso, M. Isarraraz, G. von Son, I-H. Lu, W. Michailow, B. Moller, V. Klee1, J. Mann, A. Wixforth, L. Bartels, and H. J. Krenner, *Nat. Comm.* 6, 8593 (2015).
  - <sup>19</sup> Y.-T. Liou, A. Hernández-Mínguez, J. Herfort, J.M.J. Lopes, A. Tahraoui, and P V Santos, *J. Phys. D: Appl. Phys.* 50, 464008 (2017).
  - <sup>20</sup> J. Tauc, R. Grigorovici, and A. Vancu, *phys.stat.sol* 15, 627 (1966).
  - <sup>21</sup> K. Sato and S. Adachi, *J. Appl. Phys.* 73 (2), 926 (1993).

- 
- <sup>22</sup> T. Hanada, in "Oxide and Nitride Semiconductors: Processing, Properties, and Applications", ed. T. Yao and S.-K. Hong, Springer Berlin Heidelberg (2009).
- <sup>23</sup> S. Martin, N. Baboux, D. Albertini, and B. Gautier, *Ultramicroscopy* 172, 47 (2017).
- <sup>24</sup> J.S. Speck and W. Pompe, *J. Appl. Phys.* 76, 466 (1994).
- <sup>25</sup> L.S.J. Peng, X.X. Xi, B.H. Moeckly, and S.P. Alpay, *Appl. Phys. Lett.* 83, 4592 (2003).
- <sup>26</sup> A. Bartasyte, S. Margueron, T. Baron, S. Oloiveri, and P. Boulet, *Adv. Mater. Interfaces* 1600998 (2017) and references therein.
- <sup>27</sup> J. Perrière, E. Million, W. Seiler, C. Boulmer-Leborgne, V. Craciun, O. Albert, J.C. Loulergue, and J. Etchepare, *J. Appl. Phys.* 91, 690 (2002).
- <sup>28</sup> (p 213) *Transparent Conductive Zinc Oxide: Basics and Applications in Thin Film Solar Cells*, ed. Klaus Ellmer Andreas Klein, Bernd Rech, Springer Science & Business Media (2007).
- <sup>29</sup> T. Ohsawa, K. Tsunoda, B. Dierre, C. Zellhofer, S. Grachev, H. Montigaud, T. Ishigaki, and N. Ohashi, *J. Cryst. Growth* 463, 38 (2017).
- <sup>30</sup> A. Ohtomo, M. Kawasaki, T. Koida, K. Masubuchi, and H. Koinuma, *Appl. Phys. Lett.* 72, 2466 (1998).
- <sup>31</sup> A.B.M. A. Ashrafi and Y. Segawa, *J. Vac. Sci. Technol. B* 23 (5), 2030 (2005).
- <sup>32</sup> W. L. Bond, *J. Appl. Phys.* 36, 1674 (1965).
- <sup>33</sup> M. Kawasaki, A. Ohtomo, I. Ohkubo, H. Koinuma, Z.K. Tang, P. Yu, G.K.L. Wong, B.P. Zhang, and Y. Segawa, *Mat. Sci. Eng. B* 56 (2–3), 239 (1998).
- <sup>34</sup> Sara Agrup, *Application of LIBS (Laser-Induced Breakdown Spectroscopy) for detection of gaseous species*, Lund Reports on Physics, LRAP-80, Lund (1987).
- <sup>35</sup> E. Axente, J. Hermann, G. Socol, L. Mercadier, S. A. Beldjilali, M. Cirisan, C. Luculescu, C. Ristoscu, I. Mihailescu, and V. Craciun, *J. Anal. At. Spectrom.* 29, 553 (2014).
- <sup>36</sup> V. Panella, G. Carlotti, G. Socino, L. GioVannini, M. Eddrief, K. Amimer, and C. Sebenne, *J. Phys.: Condens. Matter* 9, 5575 (1997).
- <sup>37</sup> D. M. Bagnall, Y. F. Chen, Z. Zhu, and T. Yao, *Appl. Phys. Lett.* 73, 1038 (1998).
- <sup>38</sup> O. Ambacher, J. Smart, J. R. Shealy, N. G. Weimann, K. Chu, M. Murphy, W. J. Schaff, L. F. Eastman, R. Dimitrov, L. Wittmer, M. Stutzmann, W. Rieger, and J. Hilsenbeck, *J. Appl. Phys.* 85, 3222 (1999).
- <sup>39</sup> L. Hao, Y. Li, J. Zhu, Z. Wu, F. Long, X. Liu, and W. Zhang, *J. Alloys and Compounds* 590, 205 (2014).
- <sup>40</sup> K. Nakamura and T. Hanaoka, *Jpn. J. Appl. Phys.* 32, 2333 (1993).
- <sup>41</sup> T. Shoji, K. Nakamura, and D. Yamazaki, *IEEE IUS proceedings*, 215 (2001).
- <sup>42</sup> P. Sharma, S. Kumar, and K. Shreenivas, *J. Mat. Res.* 18 (3), 545 (2003).